

# Interplay of particle size distribution and relative density in cyclic liquefaction resistance

Peter A. Adesina<sup>1,2,\*</sup> and Mahdi Taiebat<sup>1,\*\*</sup>

<sup>1</sup>Department of Civil Engineering, University of British Columbia, 6250 Applied Science Lane, Vancouver, BC, Canada

<sup>2</sup>Department of Civil and Mineral Engineering, University of Toronto, 35 St George St, Toronto, ON, Canada

**Abstract.** This study investigates the interplay of particle size distribution and relative density on the cyclic liquefaction resistance of sands using three-dimensional discrete element method simulations. Assemblies with varying coefficients of uniformity ( $C_u$ ) were prepared at two relative densities and underwent constant volume cyclic shearing at the same cyclic stress ratios until initial liquefaction. Results show a non-monotonic relationship between  $C_u$  and liquefaction resistance: an initial increase in resistance with increasing  $C_u$ , followed by a decrease beyond a critical  $C_u$  value, consistently observed at both relative densities. Micromechanical analyses demonstrate that this trend correlates with the rate of decline of the mechanical coordination number during the pre-liquefaction phase. A power-law relationship is established between the cyclic resistance and the rate of coordination number reduction, providing insight into the underlying fabric evolution mechanisms.

## 1 Introduction

Experimental studies have highlighted the influence of particle size distribution and relative density on the cyclic liquefaction resistance of sands [e.g., 1]. While these studies provide valuable insights into how these factors affect liquefaction susceptibility, they offer only a limited understanding of the underlying micromechanical mechanisms governing the observed trends. Notably, both experimental and numerical investigations have reported conflicting findings regarding how the influence of particle size distribution on liquefaction resistance varies with relative density—suggesting that the interaction between these parameters is complex and not yet fully resolved [e.g., 2, 3]. This highlights the need for micromechanically informed modeling strategies capable of capturing the role of fabric, interparticle forces, and grain-scale variability in shaping the macroscopic response.

In this study, we employ the discrete element method (DEM) to investigate the interplay between particle size distribution, characterized by the coefficient of uniformity ( $C_u$ ), and relative density ( $D_r$ ) in determining liquefaction resistance. Two series of three-dimensional assemblies were prepared at distinct relative densities, each covering a range of  $C_u$  values. The assemblies were subjected to constant-volume cyclic shearing, and their liquefaction resistance was evaluated based on the number of cycles required to trigger initial liquefaction. Micromechanical analyses, focusing on the evolution of coordination number during the pre-liquefaction phase, were also performed to clarify the underlying mechanisms. This study contributes to bridging a gap in recent DEM research by sys-

tematically examining the interaction between grading and density in influencing liquefaction resistance, and by providing micromechanical evidence to explain the observed trends.

## 2 Numerical simulation approach

The simulations were conducted using the open-source DEM particle dynamics code LIGGGHTS [4], employing soft contact laws comprising a Hertzian normal model and a history-dependent tangential model with a Coulomb friction cut-off to describe particle interactions. Assemblies of spherical particles were generated with linear gradings, each with a minimum particle diameter of  $d_{\min} = 0.50$  mm and varying maximum diameter,  $d_{\max}$ , resulting in an increasing  $C_u = d_{60}/d_{10} = 1.2$ –4.5 (Fig. 1a); higher  $C_u$  values were not considered because of the significantly increased computational cost. Two series of assemblies were prepared at distinct relative densities:  $D_r = 30\%$  and  $D_r = 50\%$ . For each  $D_r$  level, five assemblies with different  $C_u$  values were generated. The target initial void ratios were selected based on the measured minimum and maximum void ratios for each grading (Fig. 1b). Representative Elementary Volume (REV) analysis guided the number of particles: approximately 20,000 particles for  $C_u = 1.2$ –2.7, 30,000 for  $C_u = 3.6$ , and 70,000 for  $C_u = 4.5$ .

Samples were isotropically consolidated under an initial mean effective stress of  $p_0 = 100$  kPa using a four-stage sample preparation procedure following [5], modified from [6, 7]. Key simulation parameters included a particle Young's modulus of  $E = 70$  GPa, Poisson's ratio  $\nu = 0.25$ , particle density  $\rho = 2650$  kg/m<sup>3</sup>, rolling friction coefficient  $\mu_r = 0.1$ , and tangential friction coefficient  $\mu_{\text{prep}}$  during sample preparation, consistent with prior

\*e-mail: peter.adesina@utoronto.ca

\*\*e-mail: mtaiebat@civil.ubc.ca

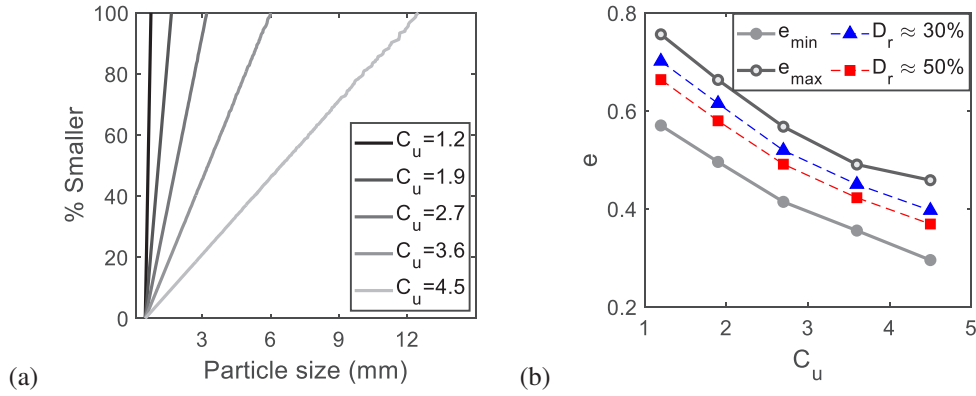


Figure 1: (a) Particle size distributions, and (b) minimum, maximum, and initial void ratios for assemblies with  $D_r = 30\%$  and  $50\%$  at different  $C_u$  values.

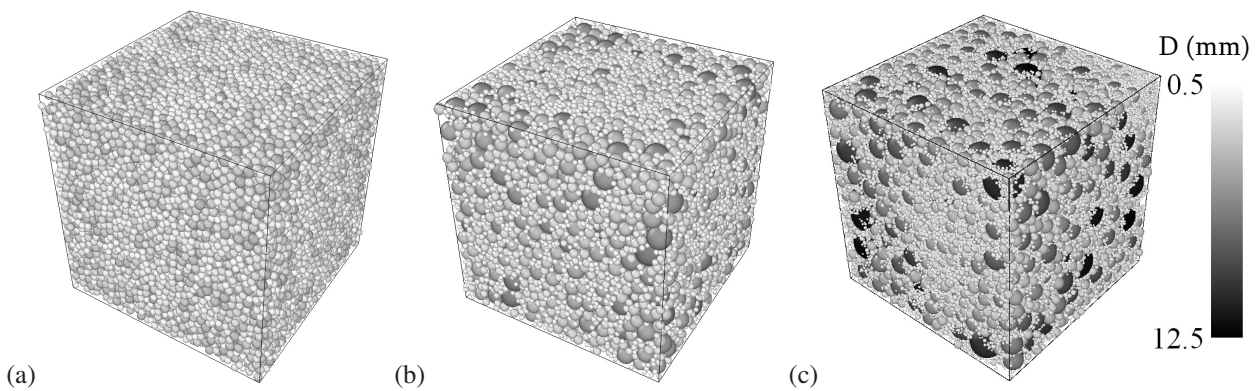


Figure 2: Snapshots of assemblies at  $D_r = 50\%$ : (a)  $C_u = 1.2$ , (b)  $C_u = 2.7$ , and (c)  $C_u = 4.5$ .

studies [8]. The value of  $\mu_{prep}$  was adjusted to achieve the target relative density, followed by setting  $\mu = 0.5$  during shearing. Fig. 2 shows snapshots of selected prepared assemblies.

After preparation, the assemblies were subjected to constant-volume cyclic simple shearing with bi-periodic lateral boundaries and rigid top and bottom boundaries. Shearing was applied by moving the top wall horizontally at a constant velocity corresponding to a shear strain rate of  $\dot{\gamma} = 1 \text{ s}^{-1}$ , ensuring a pre-liquefaction inertial number below  $10^{-3}$ . The cyclic stress ratio was set to  $CSR = 0.40$ , with the shearing direction reversed upon reaching the target shear stress [9, 10].

### 3 Macroscale data

The stress tensor for a granular assembly is computed as  $\sigma_{ij} = (1/V) \sum_{p=1}^{N_p} V^p \sigma_{ij}^p$ , where  $V^p$  and  $\sigma_{ij}^p$  are the volume and stress of individual particles, and  $V$  is the total system volume. In simple shear, the shear stress is  $\tau = \sigma_{xz}$  and the mean effective stress is  $p = (\sigma_{xx} + \sigma_{yy} + \sigma_{zz})/3$ . Deduced excess pore pressure is calculated as  $\Delta u = p_0 - p$ , with the dimensionless excess pore pressure ratio defined as  $r_u = \Delta u/p_0$ . Shear strain is computed as  $\gamma = x_w/h$ , where  $x_w$  is the cumulative horizontal displacement of the top wall. The number of cycles,  $N$ , is used as the time variable, with a cycle defined by two successive occurrences of  $\gamma = 0$ .

Figs. 3a,b illustrate typical macroscopic responses of selected assemblies during cyclic shearing. All assemblies exhibit an overall contractive response leading to liquefaction, reflected in the reduction of  $p$  from the initial 100kPa to near zero (Fig. 3a) and an increase in  $r_u$  toward unity (Fig. 3b). The number of cycles to initial liquefaction,  $N_{IL}$ , is defined as the first instance when  $r_u$  exceeds 0.95. Fig. 4 summarizes  $N_{IL}$  for all assemblies. Assemblies with  $D_r = 50\%$  consistently exhibit higher liquefaction resistance than those with  $D_r = 30\%$ , attributable to their lower initial void ratios and higher contact densities. The trend of  $N_{IL}$  with respect to  $C_u$  is similar in both series: liquefaction resistance increases with increasing  $C_u$  up to approximately  $C_u = 3.6$ , followed by a reduction at higher  $C_u$  values. This non-monotonic trend is partly consistent with the findings of [2], who observed a similar pattern at low densities but a reverse trend at higher densities. It differs, however, with the conclusion of [3], who reported higher liquefaction resistance for poorly graded specimens when compared at the same relative densities. The consistency of the non-monotonic trend observed here across both densities may be partly attributed to the relatively large assembly sizes used in this study, which ensures an adequately representative granular fabric.

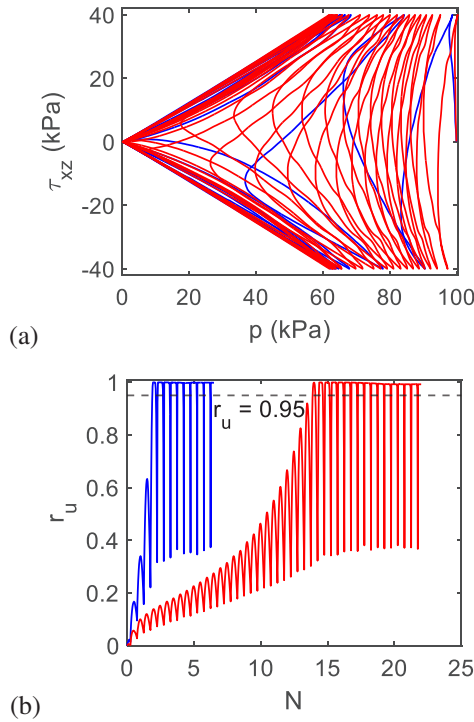


Figure 3: (a) Stress path, and (b) excess pore pressure ratio evolution for  $C_u = 2.7$  at  $D_r = 30\%$  (blue) and  $50\%$  (red).

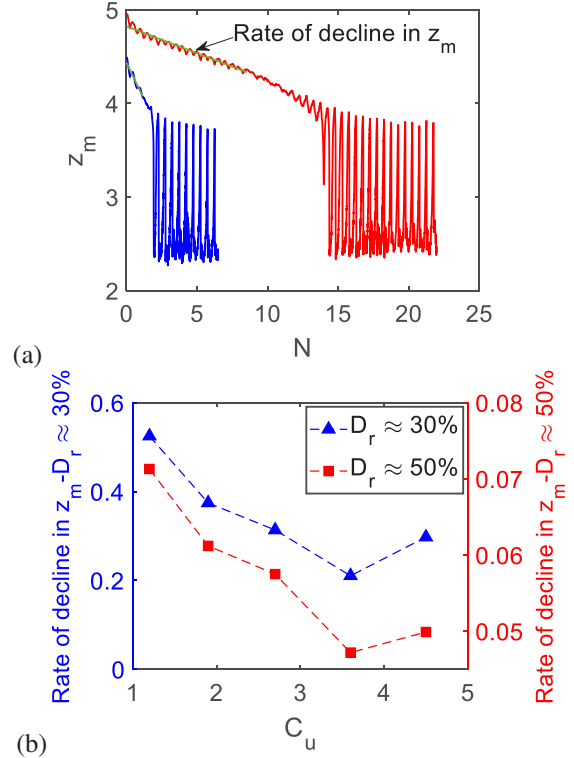


Figure 5: (a) Evolution of  $z_m$  for  $C_u = 2.7$  at  $D_r = 30\%$  (blue) and  $50\%$  (red), and (b) effect of  $C_u$  on  $\dot{z}_m$ .

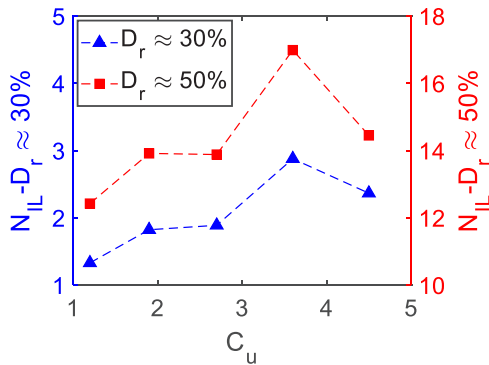


Figure 4: Effect of  $C_u$  on number of cycles to initial liquefaction for  $D_r = 30\%$  and  $50\%$ .

### 4 Micromechanical analysis

To investigate the micromechanical origins of the observed macroscale trends, we examined the evolution of the mechanical coordination number,  $z_m = (2N_c - N_p^1)/(N_p - N_p^0 - N_p^1)$ , with  $N_c$  and  $N_p$  the total number of contacts and particles, and  $N_p^0$  and  $N_p^1$  the number of particles with zero and one contact, respectively. Fig. 5a illustrates the evolution of  $z_m$  during cyclic shearing for selected assemblies with  $C_u = 2.7$  at  $D_r = 30\%$  and  $50\%$ . For both densities,  $z_m$  exhibits an approximately linear decline during the pre-liquefaction phase, followed by significant contact loss and fluctuations in the post-liquefaction phase, accompanied by large strain accumulation. The rate of decline in  $z_m$  during pre-liquefaction, denoted  $\dot{z}_m$ , was quantified as

the slope of a best-fit linear trend over this phase (green lines in Fig. 5a). Fig. 5b summarizes  $\dot{z}_m$  for all assemblies. It is observed that  $\dot{z}_m$  is strongly influenced by both  $C_u$  and  $D_r$ , with lower rates of decline associated with higher liquefaction resistance (higher  $N_{IL}$ ). Notably, the trend of  $\dot{z}_m$  with  $C_u$  mirrors the non-monotonic trend observed in  $N_{IL}$  (Fig. 4), with a minimum rate of decline at intermediate  $C_u$ .

A clear power-law relationship is established between  $N_{IL}$  and  $\dot{z}_m$  across all assemblies, regardless of relative density (Fig. 6). This correlation, which must be assessed for  $C_u > 4.5$  in the future, highlights that liquefaction re-

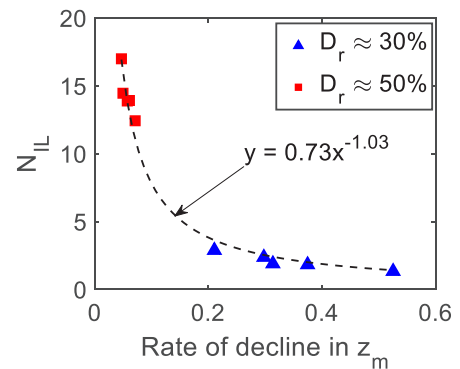


Figure 6: Number of cycles to initial liquefaction vs. rate of decline in  $z_m$  across all assemblies.

sistance is closely governed by the rate of contact loss during the pre-liquefaction phase, confirming that the interplay of particle size distribution and density systematically affects the micromechanical evolution leading to liquefaction.

## 5 Conclusion

This study examined the combined effect of particle size distribution and relative density on the cyclic liquefaction resistance of granular assemblies using DEM simulations. Assemblies prepared at  $D_r = 30\%$  and  $50\%$  consistently showed greater liquefaction resistance at higher density. For both densities, resistance increased with  $C_u$  up to about 3.6, then declined at higher  $C_u$  values. Micromechanical analysis revealed a clear correlation between resistance and the rate of decline in mechanical coordination number during pre-liquefaction, following a power-law trend. These results clarify the interplay between grading and density and offer micromechanical insight into the mechanisms governing cyclic liquefaction resistance, providing a basis for more informed interpretation of laboratory and field observations.

## Acknowledgements

Financial support for this study was provided by the Natural Sciences and Engineering Research Council of Canada (NSERC). The authors thank Prof. E.M. Rathje for facilitating access to the Texas Advanced Computing Center.

## References

- [1] Y. Vaid, J. Fisher, R. Kuerbis, D. Negussey, Particle gradation and liquefaction, *Journal of Geotechnical Engineering* **116**, 698 (1990). [https://doi.org/10.1061/\(ASCE\)0733-9410\(1990\)116:4\(698\)](https://doi.org/10.1061/(ASCE)0733-9410(1990)116:4(698))
- [2] S.K. Banerjee, M. Yang, M. Taiebat, Effect of coefficient of uniformity on cyclic liquefaction resistance of granular materials, *Computers and Geotechnics* **155**, 105232 (2023). <https://doi.org/10.1016/j.compgeo.2022.105232>
- [3] M.S. Basson, A. Martinez, J.T. DeJong, DEM simulations of the liquefaction resistance and post-liquefaction strain accumulation of coarse-grained soils with varying gradations, *Computers and Geotechnics* **174**, 106649 (2024). <https://doi.org/10.1016/j.compgeo.2024.106649>
- [4] C. Kloss, C. Goniva, A. Hager, S. Amberger, S. Pirker, Models, algorithms and validation for opensource DEM and CFD-DEM, *Progress in Computational Fluid Dynamics, an International Journal* **12**, 140 (2012). <https://doi.org/10.1504/PCFD.2012.047457>
- [5] M. Yang, M. Taiebat, P. Mutabaruka, F. Radjaï, Evolution of granular materials under isochoric cyclic simple shearing, *Physical Review E* **103**, 032904 (2021). <https://doi.org/10.1103/PhysRevE.103.032904>
- [6] C. Thornton, Numerical simulations of deviatoric shear deformation of granular media, *Géotechnique* **50**, 43 (2000). <https://doi.org/10.1680/geot.2000.50.1.43>
- [7] M.R. Kuhn, H.E. Renken, A.D. Mixsell, S.L. Kramer, Investigation of cyclic liquefaction with discrete element simulations, *Journal of Geotechnical and Geoenvironmental Engineering* **140**, 04014075 (2014). [https://doi.org/10.1061/\(asce\)gt.1943-5606.0001181](https://doi.org/10.1061/(asce)gt.1943-5606.0001181)
- [8] M. Yang, M. Taiebat, Effect of anisotropic consolidation on cyclic liquefaction resistance of granular materials via 3d-dem modeling, *Journal of Geotechnical and Geoenvironmental Engineering* **150**, 04024028 (2024). <https://doi.org/10.1061/jggef.k.gteng-11970>
- [9] M. Yang, M. Taiebat, F. Radjaï, Liquefaction of granular materials in constant-volume cyclic shearing: Transition between solid-like and fluid-like states, *Computers and Geotechnics* **148**, 104800 (2022). <https://doi.org/10.1016/j.compgeo.2022.104800>
- [10] M. Yang, M. Taiebat, P. Mutabaruka, F. Radjaï, Evolution of granular media under constant-volume multidirectional cyclic shearing, *Acta Geotechnica* pp. 1–24 (2022). <https://doi.org/10.1007/s11440-021-01239-0>